LETTER

Adaptive Local Thresholding for Co-Localization Detection in Multi-Channel Fluorescence Microscopic Images

Eisuke ITO[†a)], **Yusuke TOMARU**[†], **Akira IIZUKA**[††], **Hirokazu HIRAI**[††], ***Nonmembers***, ***and*** **Tsuyoshi KATO**[†], ***Member***

SUMMARY Automatic detection of immunoreactive areas in fluorescence microscopic images is becoming a key technique in the field of biology including neuroscience, although it is still challenging because of several reasons such as low signal-to-noise ratio and contrast variation within an image. In this study, we developed a new algorithm that exhaustively detects co-localized areas in multi-channel fluorescence images, where shapes of target objects may differ among channels. Different adaptive binarization thresholds for different local regions in different channels are introduced and the condition of each segment is assessed to recognize the target objects. The proposed method was applied to detect immunoreactive spots that labeled membrane receptors on dendritic spines of mouse cerebellar Purkinje cells. Our method achieved the best detection performance over five pre-existing methods.

key words: *co-localized spot detection, co-localization analysis, fluorescence microscopy, image processing*

1. Introduction

In the field of biology, fluorescence microscopy is widely employed to investigate the functional and morphological features of samples [1]. In the fluorescent microscopic analysis, samples are immunolabeled with antibodies bound to fluorophores, and the laser is irradiated, then the fluorescence is acquired as an image. In the *co-localization* analysis [2], multiple proteins in tissue samples are labeled with specific antibodies bound to different fluorophores, yielding a multi-channel image representing distribution and density of target proteins. In a multi-channel image, when a fluorescent spot in one channel overlaps on a spot in a different channel, it is judged that two proteins are co-localized in the same area. For quantitative analysis, co-localized regions are detected, where values, such as numbers and areas, are statistically examined. Detection of the co-localized targets in multi-channel images is often performed manually: such approaches are tedious and exhausting, and more importantly, the analysis tends to become subjective. Thus, it is required to develop unbiased analyses without heavy manual expenses. However, automated computational analysis of detection of co-localized areas in a multi-channel fluorescence image is challenging, because of several reasons such as low resolution restricted by optical properties, low signal-to-noise ratio, and contrast variation within an image [3].

Existing computational methods to detect co-localized areas can be classified into two groups: the pixel-based approach and the object-based approach [4]. Several criteria such as the Pearson's correlation coefficient (e.g. [2]) and Manders' overlap coefficient [5] have been used in the pixel-based detection of co-localization. However, these methods provide only strengths of co-localization for each pixel, which does not suffice for the subsequent quantitative analysis. Lachmanovich *et al.* [6] proposed a method that applies the top-hat transformation and watershed segmentation to each channel of the image, in order to detect the objects in each channel image. A critical shortcoming of their method would be difficulty in detecting targets in different channel images when the segments of target objects have different shapes.

Meanwhile, object-based spot detection methods exploit the prior information about the target objects to improve the detection performances. Ruusuvuori *et al.* [7] adopted the band-pass filtering (BPF) to enhance the spots and suppress shot noises generated at the image acquisition phase. The feature point detection (FPD) method proposed by Sbalzarini and Koumouysakos [8] removes the background noise with a boxcar average and enhances the spots by a convolution with a Gaussian kernel. Smal *et al.* [1] applied the h-dome transform method to detect a spot, which subtracts a constant intensity from the edge-enhanced image of the input image, and generates locally high-intensity regions. For spot detection, Olivo-Marin *et al.* [9] used multi-scale wavelets (MW) that take the product image of multiple torus wavelet transforms with different scales. The sub-pixel location (SPL) method [10] finds areas with locally maximal intensities by comparing the neighborhood intensities with the standard deviation of the background intensities. However, detection of co-localized spots by these object-based methods was primarily aimed to find spots in a single channel image.

Our goal is to develop an algorithm for co-localized object detection in multi-channel fluorescence microscopic images, where shapes of target objects are not identical in different channels. As a main application of the present method, we tried to identify membrane receptor spots im-

Manuscript received June 6, 2016.
Manuscript revised July 15, 2016.
Manuscript publicized July 27, 2016.

[†]The authors are with Department of Computer Science, Gunma University Graduate School of Science and Technology, Kiryu-shi, 376–8515 Japan.

[††]The authors are with Department of Neurophysiology & Neural Repair, Gunma University Graduate School of Medicine, Maebashi-shi, 371–8511 Japan.

a) E-mail: ito-eisuke@kato-lab.cs.gunma-u.ac.jp

DOI: 10.1587/transinf.2016EDL8118

munolabeled with a fluorophore (detected in one channel), which were present in dendritic spines of mouse cerebellar Purkinje cells, and thus, should co-localize with the dendritic spines immunolabeled with a different fluorophore (and, therefore, spines were detected in another channel). In one of the two channels, named *Channel 1* here, membrane receptors in dendritic spines are visualized, although some irrelevant noises are also contained in the channel. In another channel image, *Channel 2*, spines (and shafts of Purkinje cell dendrites) are visualized. High-intensity spots in Channel 1 without positive signals in Channel 2 can be judged as noise. Thus, in this application, the goal is to detect positive spots in Channel 1 overlapping on Channel 2 signal.

Characters of our target objects in multi-channel images are different from those of pre-existing research for co-localization analysis and spot detection for fluorescence microscopic images. Because of the aforementioned reasons, neither existing pixel-based methods nor object-based methods work well in our problem setting, and thus, we decided to develop a new algorithm suitable for our target application.

In this study, we developed a new algorithm that exhaustively detects co-localized spot regions in multi-channel fluorescence images. We tackled to properly detect different shapes in different channel images. Namely, different adaptive binarization thresholds for different local regions in different channels are introduced, and the condition of each segment is assessed to recognize the target objects. This strategy enables the proposed method to effectively handle nonhomogenous contrast images. This method was applied to detect membrane receptors in dendritic spines of mouse cerebellar Purkinje cells. The detection performance of this method was assessed by comparing with the five above mentioned, pre-existing methods for spot detection: BPF [7], FPD [8], HD [11], MW [9], SPL [10].

2. Method

We developed a new computational method for spot detection from multi-channel fluorescence microscopic images. Our method was designed to effectively detect co-localized spots even if the shape of the fluorescence in one channel is dissimilar to the one in another channel.

In the proposed method, each channel image is binarized with some threshold, and the logical product of them is taken. For each connected component in the logical product image, the proposed method examines whether the connecting component in the local region satisfies the condition as a target object. A prominent feature of the proposed method is to adjust the threshold for binarization in each local region. Figure 1 shows a typical example of how the proposed method determines the binarization thresholds adaptively. In this figure, we consider a single channel image for simplicity. If the value t_a is used as the binarization threshold, the segment obtained is too large as a target spot in the local region. When the threshold is increased to t_b, two segments appear. The shape and the size of the right segment are acceptable as a target object, and thus, the threshold of the right segment is determined to t_b. The size and shape of the left segment are satisfied as a target object when the threshold is increased to t_c. Accordingly, the threshold of the left segment is determined to t_c. Thus, the local binarization thresholds are determined adaptively by examining whether the size and shape obtained with a certain threshold match a category of a target object. In the next subsection, detection algorithm designed from these ideas is presented.

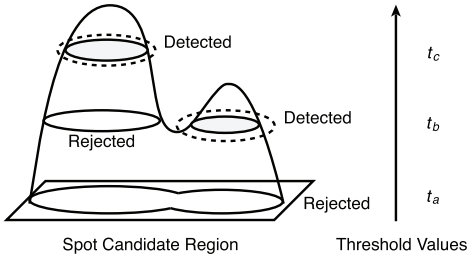

Fig. 1 Adaptive selection of a threshold value for each segment.

2.1 Algorithm

The flowchart of the algorithm in two channels is shown in Fig. 2. Suppose that an N-channel fluorescence microscopic image and N different initial binarization thresholds are given, then, each process is as follows:
(S1) *Binarization* step: Each channel image is binarized with the respective threshold, and then the logical product of N different binarized images is taken.
(S2) *Segment extraction* step: Noise of the logical product image is removed by morphological dilation followed by erosion, and all connected components (referred to as *segments* hereinafter) are enumerated.
(S3) *Judgement* step: The contour of the segment is extracted to judge whether the extracted segment fall within the criteria for a target object, which is defined in Sect. 2.2. If the segment fits the criteria, the contour is recognized as a target object.
(S4) *Threshold update* step: The binarization threshold is increased by adding a pre-defined small value. Then, using a new threshold, repeat the three steps (S1)–(S3) for the segments rejected in the previous step.

Note that this algorithm is recursive. At the first attempt, the binarization at (S1) is global; it is applied to the entire image. After returning from (S4), subsequent binarization is local; it is applied to the restricted image within the segment rejected at (S3) in the previous trial.

Our proposed method does not detect or correct the signal crosstalk or bleed-through. Therefore, the combination of fluorophores and filter sets should be selected carefully, or a preprocessing method such as signal unmixing should be applied to prevent those problems [12]. Our method assumes that the signals among the channels are independent.

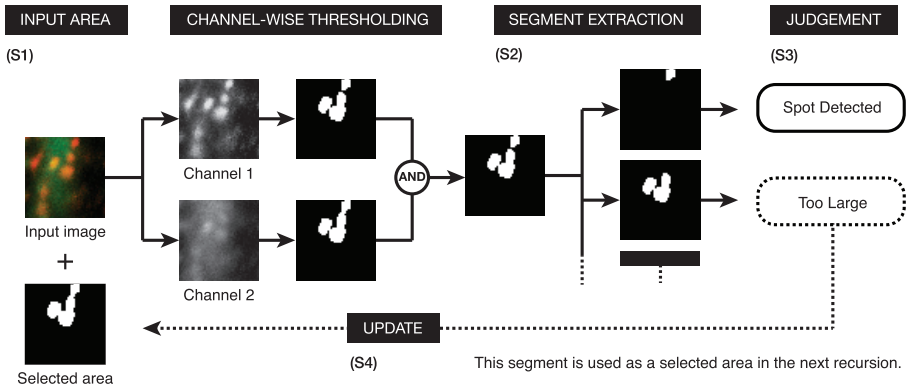

Fig. 2 Outline of the proposed method. (S1) First, an input multi-channel image (an overlayed image immunoreactive to different proteins) and the pre-defined area are provided. Then, the input multi-channel image is separated into each channel and binarized using respective thresholds, and the logical product is obtained within the selected area. (S2) The logical product image is de-noised, and all connected components are extracted. (S3) Each component is discriminated by using the condition consisting of the area and the ellipticity. (S4) If a connected component does not meet the condition, go back to and repeat the step S1 using a new threshold to which a pre-defined gain is added.

2.2 Target Object Criteria

Step (S3) judges whether the segments that fall within the criteria contains only a single target object. An example used for verification of the present method is detection of membrane receptors in dendritic spines of Purkinje cells, which have a round shape with almost a similar size. Therefore, the area and the ellipticity are used for the judgement. Namely, a segment is recognized as a target object if the following two conditions are satisfied, where the area and the ellipticity are denoted by S_j and c_j, respectively:

- $S_{\min} \leq S_j \leq S_{\max}$, and
- $c_j \leq c_{\max}$.

Therein, $S_{\min}$, $S_{\max}$, and $c_{\max}$ are constant. If $S_j < S_{\min}$, the segment is judged as a noise, and discarded. If $S_{\max} < S_j$, the segment may contain multiple target objects, as explained in Fig. 3. The ellipticity c_j is the ratio of major radius to minor radius of the ellipse that approximates the segment. If $c_{\max} < c_j$, the segment is not likely to be a right target object because it contradiiects the assumption that the shape of the target is round.

2.3 Example

An example of the two-channel microscopic image is shown in Fig. 3 (a), where two channels are assigned to red and green colors for visualization. Here we focus on the small square region in Fig. 3 (a), which is enlarged to Fig. 3 (b). First, each channel image is binarized using respective initial thresholds. After de-noising from the resultant logical products, all connected components (segments) are extracted, followed by evaluation whether the extracted segments fit the criteria for target images. In the condition described in Sect. 2.2, the segment in a magenta rectangle in Fig. 3 (e) is too large as a target object, and therefore, the threshold for binarization is increased for re-binarization. Then, as shown in Fig. 3 (g), the large segment is divided into two segments. The green segment in Fig. 3 (h) satisfies the object criteria, whereas another segment does not. This recursive binarization process is repeated for another segment. Eventually, four target objects are obtained from the region initially recognized as one object, as shown in Fig. 3 (j).

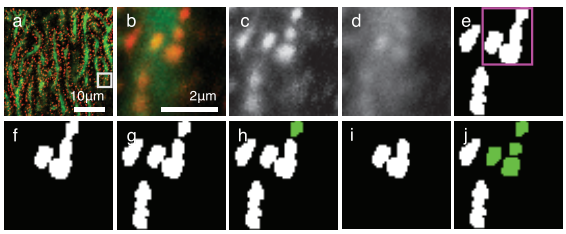

Fig. 3 Examples of the co-localization detection. (a) An input two-channel image. (b) Enlarged image of a small rectangle region in (a). (c)–(j) Panels showing the process of the co-localization detection through the recursive binarization steps. Panels (c) and (d) are color channels corresponding to different fluorophores. Panels (f) and (i) are the selected areas that were rejected segments in a previous round of recursive processing.

Table 1 Performances of the proposed method (Ours) as well as pre-existing methods. Two-channel fluorescent microscope images (total 18 images) were analyzed. The averages and standard deviations are presented.

	Detection Score		
	Precision	Recall	F-score
BPF [7]	0.708 ± 0.13	0.811 ± 0.07	0.750 ± 0.09
FPD [8]	0.742 ± 0.11	0.788 ± 0.04	0.762 ± 0.08
HD [11]	0.611 ± 0.12	0.718 ± 0.07	0.655 ± 0.09
MW [9]	0.726 ± 0.11	0.747 ± 0.10	0.732 ± 0.10
SPL [10]	0.775 ± 0.14	0.651 ± 0.08	0.696 ± 0.07
Ours	**0.789 ± 0.06**	**0.814 ± 0.09**	**0.796 ± 0.05**

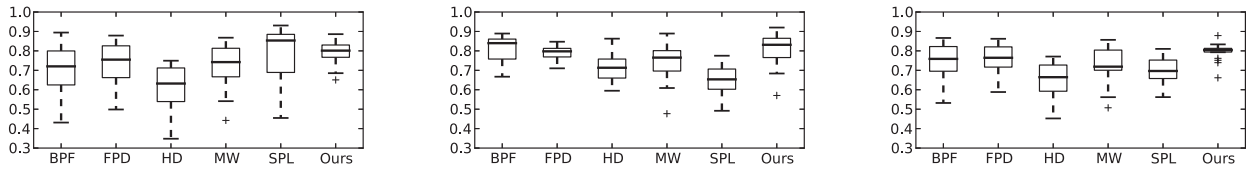

(a) Precision (b) Recall (c) F-score

Fig. 4 Box plots showing Precisions (a), Recalls (b), and F-scores (c) for spot detection, which were obtained using 18 two-channel fluorescent images. The results were obtained by five pre-existing methods (BPF [7], FPD [8], HD [11], MW [9], SPL [10]) and the proposed method (Ours).

3. Experiments

To verify the performance of the present method, we conducted simulations that detect membrane receptors on dendritic spines of Purkinje cells. In this section, we compared our new method with five pre-existing methods, BPF [7], FPD [8], HD [11], MW [9], and SPL [10]. The dataset used for the comparison was obtained using a protocol previously reported by Iizuka *et al.* [13]. Briefly, parasagittal sections of mouse cerebellar vermis were double immunolabeled for the calcium binding protein (Calbindin D-28K, a marker for Purkinje cell) and the delta2 glutamate receptor (GluD2). Immunoreactive fluorescent images of Calbindin D-28K and GluD2 were acquired by using a confocal laser microscope (LSM 5 PASCAL; Zeiss). Here, one signal was from Alexa Fluor 488, and the other was from Alexa Fluor 568. Filter sets were selected properly to prevent bleed-through of the signals. This dataset was obtained from 18 fluorescent images from six mice (three images/mouse). Our targets of detection are spot-like regions immunoreactive to GluD2 overlapped on immunoreactivity of Calbindin D-28K. As a ground truth, experts in this field manually annotated the correct GluD2 spots.

In the present trial, for the channel-wise binarization step, we set an initial threshold to 30 for GluD2, and to 10 for Calbindin, respectively. For the judgement step, we selected the maximum ellipticity ($c_{\max}$) to 2.0, the minimum area ($S_{\min}$) to 3, and the maximum area ($S_{\max}$) to 400. For each pre-existing method, optimal parameters for this dataset were experimentally decided.

For quantitative assessment of detection performance of target objects, we employed Precision, Recall, and F-score. Those scores depend on the numbers of true positives (TP), false positives (FP), and false negatives (FN): TP is a correctly detected object, whereas FP is an incorrectly detected object without a ground truth on its position, and FN is an undetected object in spite of a presence of a ground truth. We determined the Precision, Recall, and F-score in all 18 two-channel images. Table 1 shows the averages and standard deviations of those scores. As the results indicate, our method was superior to all five pre-existing methods in every evaluation index. Figure 4 shows the box plots of the Precision, Recall, and F-scores, which were obtained by our and pre-existing methods using 18 two-channel images of GluD2 and Calbindin. In contrast to the large variances in the pre-existing methods, the results obtained using our method showed much less variances, suggesting that the proposed method is most stable and resistant to the variations during image acquisition.

4. Conclusion

In this paper, we presented a new computational method for high-throughput detection of co-localized spots in multi-channel fluorescence microscopic images. The proposed method is superior to the existing methods in terms of the ability to detect objects whose shapes are different among the multiple channels. We verified the performance of this method by detecting membrane receptors (GluD2) expressed in dendritic spines of mouse cerebellar Purkinje cells. The results obtained using the real experimental data revealed that the proposed method achieved the best performance over all five pre-existing methods. Further verification using different types of experimental data is needed to warrant the reliable quality and possible application of the proposed method.

References

[1] I. Smal, M. Loog, W. Niessen, and E. Meijering, "Quantitative comparison of spot detection methods in fluorescence microscopy," IEEE Trans. Med. Imag., vol.29, no.2, pp.282–301, 2010.

[2] A.L. Barlow, A. MacLeod, S. Noppen, J. Sanderson, and C.J. Guérin, "Colocalization analysis in fluorescence micrographs: Verification of a more accurate calculation of Pearson's correlation coefficient," Microscopy and Microanalysis, vol.16, no.6, pp.710–724, Dec. 2010.

[3] J.C. Waters, "Accuracy and precision in quantitative fluorescence microscopy," The Journal of Cell Biology, vol.185, no.7, pp.1135–1148, 2009.

[4] T. Lagache, N. Sauvonnet, L. Danglot, and J.-C. Olivo-Marin, "Statistical analysis of molecule colocalization in bioimaging," Cytometry Part A, vol.87, no.6, pp.568–579, 2015.

[5] E.M.M. Manders, F.J. Verbeek, and J.A. Aten, "Measurement of co-localization of objects in dual-colour confocal images," Journal of Microscopy, vol.169, no.3, pp.375–382, 1993.

[6] E. Lachmanovich, D.E. Shvartsman, Y. Malka, C. Botvin, Y.I. Henis, and A.M. Weiss, "Co-localization analysis of complex formation among membrane proteins by computerized fluorescence microscopy: Application to immunofluorescence co-patching studies," Journal of Microscopy, vol.212, no.2, pp.122–131, 2003.

[7] P. Ruusuvuori, T. Äijö, S. Chowdhury, C. Garmendia-Torres, J. Selinummi, M. Birbaumer, A.M. Dudley, L. Pelkmans, and O. Yli-Harja, "Evaluation of methods for detection of fluorescence labeled subcellular objects in microscope images," BMC Bioinfor-

matics, vol.11, no.1, pp.1–17, 2010.

[8] I.F. Sbalzarini and P. Koumoutsakos, "Feature point tracking and trajectory analysis for video imaging in cell biology," Journal of Structural Biology, vol.151, no.2, pp.182–195, 2005.

[9] J.-C. Olivo-Marin, "Extraction of spots in biological images using multiscale products," Pattern Recognit., vol.35, no.9, pp.1989–1996, 2002.

[10] K. Jaqaman, D. Loerke, M. Mettlen, H. Kuwata, S. Grinstein, S.L. Schmid, and G. Danuser, "Robust single-particle tracking in live-cell time-lapse sequences," Nature Methods, vol.5, no.8, pp.695–702, 2008.

[11] J.C. Crocker and D.G. Grier, "Methods of digital video microscopy for colloidal studies," Journal of Colloid and Interface Science, vol.179, no.1, pp.298–310, 1996.

[12] T. Zimmermann, "Spectral imaging and linear unmixing in light microscopy," Microscopy Techniques, Advances in Biochemical Engineering/Biotechnology, vol.95, pp.245–265, Springer, 2005.

[13] A. Iizuka, Y. Matsuzaki, A. Konno, and H. Hirai, "Plasticity of the developmentally arrested staggerer cerebellum in response to exogenous RORα," Brain Structure and Function, vol.221, no.6, pp.2879–2889, 2016.